# Energetics and ionization dynamics of two diarylketone molecules: benzophenone and fluorenone

Zied Gouid, Anja Röder, Barbara Cunha de Miranda, Marc-André Gaveau, Marc Briant, Benoît Soep, Jean-Michel Mestdagh, Majdi Hochlaf, Lionel Poisson

PCCP

PAPER

View Article Online
View Journal | View Issue



Cite this: *Phys. Chem. Chem. Phys.*, 2019, **21**, 14453

# Energetics and ionization dynamics of two diarylketone molecules: benzophenone and fluorenone†

Zied Gouid,[a] Anja Röder,[‡bc] Barbara K. Cunha de Miranda,[b] Marc-André Gaveau,[b] Marc Briant,[b] Benoît Soep,[b] Jean-Michel Mestdagh,[b] Majdi Hochlaf *[a] and Lionel Poisson *[b]

Single photon ionization and subsequent unimolecular ion decomposition were studied on jet-cooled benzophenone and fluorenone separately, using VUV synchrotron radiation in a photoion/photoelectron coincidence setup. Slow PhotoElectron Spectra (SPES) were recorded in coincidence with either the parent or the fragment ions for $h\nu < 12.5$ eV. Dissociative ionization is observed for benzophenone only. The full interpretation of the measurements, including the identification of the neutral and ionic species when dissociative ionization is at play, benefits from high level *ab initio* computations for determining the equilibrium structures and the energetics of the neutral and ionized molecules and of their fragments. Electronically excited states of the parent molecular ions were calculated also. From this analysis, an accurate experimental determination of the energetics of the benzophenone and fluorenone ions and of their fragmentation channels is available: adiabatic ionization energies of benzophenone at 8.923 ± 0.005 eV and of fluorenone at 8.356 ± 0.007 eV; and appearance energies of benzophenone fragment ions at 11.04 ± 0.02 eV (loss of $C_6H_5$), 11.28 ± 0.02 eV (loss of H) and 11.45 ± 0.02 eV (loss of CO). The corresponding fragmentation mechanisms are explored, showing likely concerted bonds rearrangement. Possible pre-ionizing fragmentation is discussed in light of the spectra presented. The structural rigidity of fluorenone diarylketone seems to be the origin of the inhibition of the fragmentation of its cation.

Received 26th April 2019,
Accepted 6th June 2019

DOI: 10.1039/c9cp02385b

rsc.li/pccp



## 1 Introduction

The benzophenone molecule, a diarylketone (Fig. 1a), is a paradigmatic organic molecule where the singlet-to-triplet energy transfer is especially efficient.[1–3] The floppy character of this molecule plays a significant role in this behaviour, which is dramatically perturbed when a more rigid diarylketone molecule, such as fluorenone (Fig. 1b), is considered.[4,5] Current theoretical approaches have the power to provide information on the dynamics of such medium size organic molecules. For example, Favero *et al.*[6] confirmed the above experimental intuition and showed that the $S_1 \rightarrow T_1$ relaxation is driven by an out-of-plane deformation of the benzophenone molecule.

Out-of-plane deformations are taking place in the benzophenone cation also. They are the origin of a complex vibrational structure, revealed by photoelectron spectroscopy[7] and Slow PhotoElectron Spectroscopy (SPES).[8] These deformations likely stimulate fragmentation of the benzophenone cation when enough excess energy is available. To our knowledge, these dissociative photoionization channels have not been documented yet using the SPES technique, although this technique proved its efficiency to

[a] *Université Paris-Est, Laboratoire Modélisation et Simulation Multi Echelle, MSME UMR 8208 CNRS, 5 bd Descartes, 77454 Marne-la-Vallée, France. E-mail: majdi.hochlaf@u-pem.fr*
[b] *LIDYL, CEA, CNRS, Université Paris-Saclay, CEA Saclay, 91191 Gif-sur-Yvette, France. E-mail: lionel.poisson@cea.fr*
[c] *Institute of Physical and Theoretical Chemistry, University of Würzburg, Am Hubland, D-97074 Würzburg, Germany*

† Electronic supplementary information (ESI) available: Details of the theoretical calculations. See DOI: 10.1039/c9cp02385b

‡ Current address: Department of Chemistry, University of Ottawa, 150 Louis Pasteur, Ottawa, Ontario, K1N 6N5, Canada.

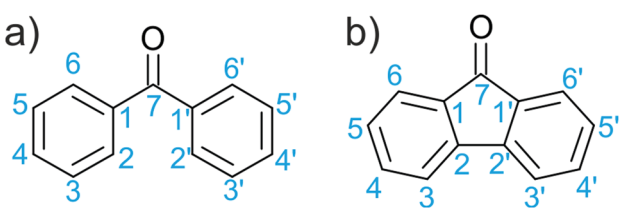


Fig. 1 (a) Benzophenone and (b) fluorenone. The numbers identify the C atoms.

unravel complex photodissociation dynamics, in particular when autoionizing states are involved.[9–11]

This lack of information has motivated the present work. All the refinement of the SPES technique was used to investigate and compare the photoionization channels of the fluorenone and benzophenone molecules, up to the fourth excited state of each cation. An intricate situation was expected where electronic and geometrical degrees of freedom are coupled. High level theoretical information is therefore needed to help unravel the resulting complex dynamics. This was achieved using a recent combined experimental–theoretical approach that proved its efficiency for unravelling the specific isomer/tautomer cytosine photoionization.[12] It proposes a good compromise between accuracy and computational capacity.[11] The calculation scheme adopted here associates: (i) optimization of molecular structures at the PBE0 level; (ii) single point energy calculations using the (R)CCSD(T)-F12 technique on the optimized structures to take the electron correlation into account; and (iii) combination of points (i) and (ii) with IC-MRCI excited state calculations.

Through this association between theory and experiment we were able to determine the adiabatic ionization energies of benzophenone and fluorenone, the vertical excitation energies of their cations and, for benzophenone, the appearance energies of the photoionization fragments. We also propose a plausible mechanism for the dissociative photoionisation of benzophenone. For fluorenone, when $h\nu < 14.0$ eV, no unimolecular fragmentation is observed.

# 2 Technical section

## 2.1 Experimental section

The experiments were performed at the French synchrotron facility SOLEIL on the DESIRS beamline.[13] The SAPHIRS setup[14] was coupled with the DELICIOUS III double imaging ion/electron coincidence spectrometer.[15]

DESIRS is an undulator based beamline. It delivered a photon beam, which passed through an argon gas filter to select photons with energy lower than 15.7 eV. The transmitted beam was dispersed by a 200 grooves per mm monochromator. The latter operated with input and output slits of 100 mm or 200 mm width, depending on the photon flux. In the present work, the energy resolution of the photons was typically 7.5 meV.

The SAPHIRS setup delivered a cw molecular beam, which crossed the photon beam at a right angle. Here, benzophenone or fluorenone molecules were carried into the molecular beam after evaporation in a home-built oven heated to $T = 100$ °C for benzophenone and $T = 185$ °C for fluorenone. These molecules were ordered from Sigma-Aldrich and used without further purification.

The photoions and photoelectrons produced by the benzophenone or fluorenone/photon interaction were extracted and imaged by the DELICIOUS III spectrometer, perpendicularly to the plane defined by the molecular and photon beams. DELICIOUS III was configured to allow us to perform an $i^2$PEPICO experiment.[16] Accordingly, the photoion signal provided the mass distribution of the photoions and the photoion/photoelectron coincidence correlated the photoions of a specific mass with the velocity map image, *i.e.* the angular and energy distributions, of the corresponding photoelectrons. An experiment consisted of recording a series of correlated photoion/photoelectron events while scanning the photon energy with the beamline monochromator.

The treatment of each raw photoelectron image included the recovery of image distortion, pBASEX[17] inverse Abel transformation and false coincidence subtraction. This allowed us to construct a 3D-plot where the photoelectron intensity and energy are plotted as a function of the photon energy. Ultimately, summation of the 3D-plot along the linear regression line relating the photoelectron and photon energies led to the Slow PhotoElectron Spectrum (SPES).[9,10] For convenience, the 3D-plot that was used to generate the SPES is called the SPES matrix.

The SPES reflects the photoionization cross-section for producing ions of a specific mass with electrons close to zero kinetic energy. Two kinds of SPESs are discussed below. Those where the photoelectrons are correlated with a specific ion, the parent ion or one of its fragments, are called an action-SPES. When summing all the photoelectrons, disregarding that they are correlated with the parent or the fragment ions, a full-SPES is obtained, which is the sum of all the action-SPESs.

The extracting field in DELICIOUS III was set to 53 V cm$^{-1}$. This led to a shift of $-5.5$ meV of the photoelectron energies, which is taken into account below when estimating the energy thresholds.[18]

## 2.2 Theoretical methods

Three series of computations were performed: (i) the equilibrium structures of neutral benzophenone and fluorenone molecules, of their ions and of several ionic fragments were determined. The electronic problem was solved using the PBE0 density functional[19] as implemented in GAUSSIAN09,[20] the atoms being described by the augmented correlation-consistent aug-cc-pVDZ basis set.[21,22] Full geometry optimizations were performed within the $C_1$ point group. The computed harmonic frequencies are all positive, indicating that the stationary points found at the optimization step are minima on the corresponding potential energy surfaces. Finally, the zero point vibrational energy correction (ZPE) was calculated at the anharmonic level after scaling the harmonic frequencies. The scaling factor is 0.9610, as recommended by Tantirungrotechai *et al.*[23]

(ii) The energy of the previously optimized structure was calculated by a single point computation using the MOLPRO suite of programs.[24] The explicitly correlated coupled cluster with single, double and perturbative triple excitations ((R)CCSD(T)-F12)[25–28] was used together with the aug-cc-pVDZ basis set in conjunction with the corresponding resolutions of the identity and density fitting functions.[29]

In a series of benchmarks where computational and experimental results are compared, we showed that the composite scheme PBE0/aug-cc-pVDZ(opt)//(R)CCSD(T)-F12/aug-cc-pVDZ(SP) allows accurate derivation of adiabatic ionization energies of medium-sized molecular systems (to within $\pm 0.01$ eV).[11,12,30–34]

 

This expected accuracy must be kept in mind in the forthcoming discussion.

(iii) The electronically excited states of the benzophenone and fluorenone cations were calculated, again using the MOLPRO package. These single point computations were performed either at the equilibrium geometry of the cation or at that of the neutral molecule. The state-averaged complete active-space self-consistent field (SA-CASSCF) technique was used,[35,36] followed by the Internally Contracted Multi Reference Configuration Interaction (IC-MRCI) approach.[37–39] The SA-CASSCF computations were conducted with an active space of 9 molecular orbitals ranging from HOMO−3 to LUMO+4; the core orbitals and the valence orbitals up to HOMO−4 were considered as closed. In the IC-MRCI computation, all configurations with coefficients larger than 0.05 in the expansion of the CASSCF wavefunctions were used as reference states. We used the MOLPRO state averaging procedure at CASSCF where we asked for four doublet states. Again, the atoms were described using the aug-cc-pVDZ basis set.

# 3 Results

## 3.1 Mass spectra

Mass spectra collected after single photoionization of benzophenone (resp. fluorenone) are shown in Fig. 2 for several photon energies within the 9.0–12.5 eV (resp. 8.5–14.0 eV) scanning range.

The benzophenone and fluorenone molecules were investigated in two different runs using different sets of experimental parameters. This appears prominently in the mass resolution when comparing the peak profiles in the spectra of the top (fluorenone) and bottom (benzophenone) panels of Fig. 2. The mass resolution was $\frac{\Delta m}{m} = 0.12\%$ and 0.5% in the fluorenone and benzophenone experiments, respectively. The fine structure which is resolved in the fluorenone spectra fits with that expected from the natural $^{13}C/^{12}C$ isotope ratio.

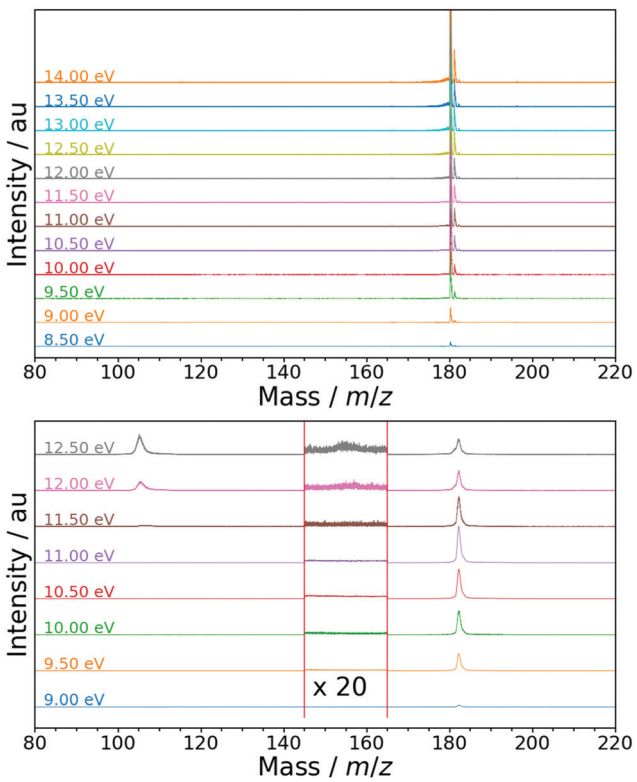


Fig. 2 Mass spectra as a function of the photon energy in the fluorenone (top panel) and benzophenone (bottom panel) experiments.

Let us first concentrate on the fluorenone mass spectra in the top panel of Fig. 2. Whatever the photon energy, only the parent mass appears. Nevertheless, a low intensity tail, close to the limit of detection, appears at the bottom of the low energy wing (left hand side) of the parent peak when the photon energy is increased. Such a broad asymmetric shape suggests delayed fragmentation during the ion flight rather than the loss of a H atom before extraction of the cation. The kinetics of this fragmentation could be documented when following the treatment detailed in ref. 40. However, this was not attempted in the present context given the very low intensity of the tail.

A qualitative difference is observed in Fig. 2 when comparing the benzophenone mass spectra (bottom panel) to those of fluorenone (top panel). At increasing photon energy, peaks at 181 u (at the limit of the mass resolution) and 106 u appear in the mass spectra of benzophenone below the parent peak at 182 u. A broad, extremely weak peak appears also, spanning over about 5 u at 154 u. The mass peaks at 181 and 106 u correspond to the loss of a H atom and a phenyl group, respectively. The broad peak centered at 154 u suggests a loss of the CO group in a complex fragmentation dynamics which converts a lot of the available energy into kinetic energy of the fragments. Again, its low signal prevents us from attempting a treatment of the fragmentation kinetics.

## 3.2 Slow photoelectron spectra (SPES)

**Benzophenone.** Two full-SPESs and one action-SPES of benzophenone are presented in Fig. 3. The low photon energy

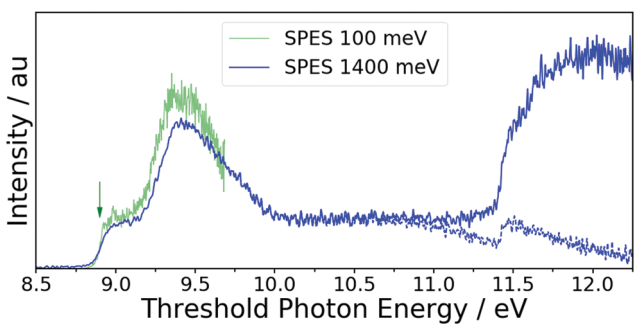


Fig. 3 Full- and action-SPESs of benzophenone: the green curve, a full-SPES, partly appears in ref. 8. It was obtained when limiting the photoelectron signal to electron energies below 0.1 eV in the SPES-matrix projection. The full blue curve uses the same raw data but the upper photoelectron energy is limited to 1.4 eV for generating the full-SPES. The dashed blue curve reports an action-SPES when further limiting the photoelectrons to those in coincidence with the parent ion. The green arrow shows the adiabatic ionization energy from the PBE0/aug-cc-pVDZ(opt)//(R)CCSD(T)-F12/aug-cc-pVDZ(SP) calculation.

part, below 11 eV, has been published already.[8] The entire energy range is shown here. The green one, a full-SPES, was constructed by considering photoelectrons of energy smaller than 0.1 eV when projecting the SPES-matrix. The spectrum shown as a full blue curve was obtained from the same raw data, but photoelectron energies up to 1.4 eV were considered in the projection. It reproduces the spectrum collected by McAlduff and Bunbury using a He–I photoelectron spectrometer.[41] Although these two previous spectra do not have exactly the same shape at low energy, they exhibit the same threshold. For comparison, the green arrow shows the adiabatic ionization energy of benzophenone, which is predicted by the present PBE0/aug-cc-pVDZ(opt)//(R)CCSD(T)-F12/aug-cc-pVDZ(SP) calculation.

The action-SPES, shown as a dashed blue curve in Fig. 3, is obtained when restricting the photoelectrons of energy below 1.4 eV to those that are in coincidence with the parent benzophenone ion. Importantly, the present full- and action-SPESs (full and dashed blue curves in Fig. 3) run together below $\approx$11 eV and look very different above. A sharp monotonic increase is observed in the full-SPES near $h\nu = 11.421 \pm 0.010$ eV whereas a Fano-like profile centered at the same energy appears in the action-SPES.

A series of action-SPESs are shown in Fig. 4, one for each benzophenone ion fragment that appears in Fig. 2. All exhibit a threshold behaviour close to the dashed red line (11.421 eV) located at the threshold that has been observed in Fig. 3. An accurate determination of the corresponding thresholds, *i.e.* appearance energies of the fragments, is provided below.

**Fluorenone.** The full-SPES spectrum of fluorenone is displayed in Fig. 5 over the photon energy range 8.2–11.0 eV. It was measured up to 14.2 eV with a lower resolution (not presented here). A technical difficulty had to be taken into account for this run. The centre of the position sensitive detector was lacking sensitivity. The corresponding underestimated counting rate at the center of the raw images was responsible for an unrealistic negative intensity of the low energy photoelectrons in the Abel inverted images. Hence, photoelectrons of energy lower than 40 meV were not included in the projection when constructing the fluorenone SPES from the SPES matrix. This is an advantage provided by the SPES method, nevertheless at the expense of a loss of resolution in the spectrum because in the SPES matrix the energy resolution decreases when the photoelectron energy increases. The spectrum shown in Fig. 5 was obtained after summing up electrons over the kinetic energy range 40–120 meV. This spectrum looks very different from the full-SPES of benzophenone presented above in Fig. 3. Three well separated bunches of unresolved bands are observed in the full-SPES of fluorenone whereas overlapping structures prevail in the benzophenone SPES.

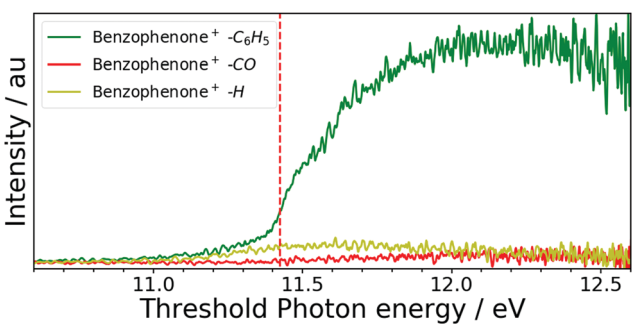


Fig. 4 Action-SPESs documenting the fragmentation channels where the benzophenone ion has lost either a $C_6H_5$ (green curve), a CO (red) or a H (dark yellow) group. The SPESs were constructed by considering the photoelectron energies in the range 0–1.4 eV when projecting the SPES-matrix. The vertical dash red line at 11.421 eV indicates the steep increase observed in the full blue curve in Fig. 3.

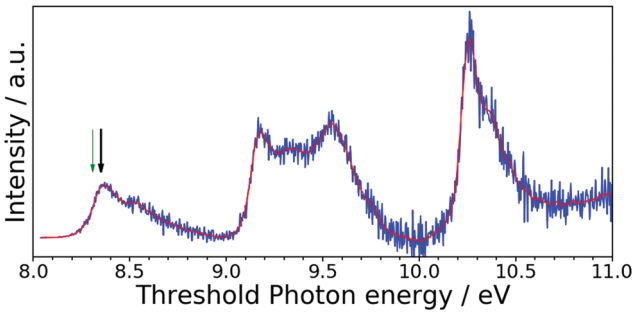


Fig. 5 Full-SPES of fluorenone, generated by considering the photoelectrons in the 40–120 meV range of kinetic energy: experimental data (blue) and smoothed curve (red) of the experimental data. The arrows show the adiabatic ionization energy either from experiment (black arrow) or from the PBE0/aug-cc-pVDZ(opt)//(R)CCSD(T)-F12/aug-cc-pVDZ(SP) calculations (green arrow).

### 3.3 Optimized geometries

**Benzophenone.** The structural properties of neutral and ionic benzophenone in their ground electronic state have been reported already.[8] Briefly, neutral benzophenone belongs to the $C_2$ point group. It is non-planar with a twist angle of 28 degrees for the phenyl groups. A low torsional frequency of 43 $cm^{-1}$ indicates a non rigid character of the molecule with respect to the $C-\widehat{CO}-C$ torsion. Just as the neutral molecule, the benzophenone cation is non-planar and non-rigid with respect to the same torsion. In contrast with neutral benzophenone, it does not have a $C_2$ but a $C_1$ symmetry, as the CO is closer to one ring than the other one. The above-mentioned angle is roughly the same, but the CO bond is now in the plane with its closest phenyl ring.

**Fluorenone.** The optimized structure of ground state fluorenone and that of the fluorenone cation are shown in Fig. 6. Both structures belong to the $C_{2v}$ point group. Several bond distances and angles are listed in Table 1.

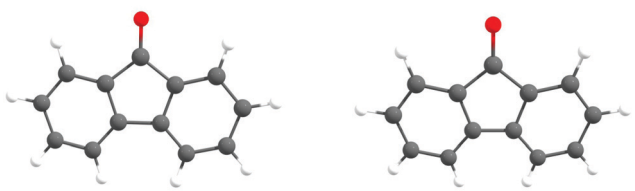

Fig. 6 Equilibrium geometries of the ground electronic state of neutral (left) and cationic (right) fluorenone after optimization at the PBE0/aug-cc-pVDZ level.

Table 1 Bond distances and bond angles defining the equilibrium geometries of the ground state fluorenone molecule and of its cation shown in Fig. 6. The numbering of the C-atoms is that defined in Fig. 1

| Bond length (Å) | Neutral | Cation |
|---|---|---|
| $C_1$–$C_7$ | 1.495 | 1.496 |
| $C_{1'}$–$C_7$ | 1.495 | 1.496 |
| $C_7$═O | 1.213 | 1.205 |
| $C_1$–$C_2$ | 1.405 | 1.432 |
| $C_{1'}$–$C_{2'}$ | 1.405 | 1.432 |
| $C_2$–$C_3$ | 1.388 | 1.409 |
| $C_{2'}$–$C_{3'}$ | 1.388 | 1.409 |
| $C_3$–$C_4$ | 1.400 | 1.382 |
| $C_{3'}$–$C_{4'}$ | 1.400 | 1.382 |
| $C_4$–$C_5$ | 1.396 | 1.414 |
| $C_{4'}$–$C_{5'}$ | 1.396 | 1.414 |
| $C_5$–$C_6$ | 1.398 | 1.405 |
| $C_{5'}$–$C_{6'}$ | 1.398 | 1.405 |
| $C_6$–$C_1$ | 1.385 | 1.373 |
| $C_{6'}$–$C_{1'}$ | 1.385 | 1.373 |
| $C_{2'}$–$C_{2'}$ | 1.480 | 1.433 |
| **Angle (deg)** | **Neutral** | **Cation** |
| $C_1 - \widehat{C_7} - O$ | 127.4 | 127.7 |
| $C_{1'} - \widehat{C_7} = O$ | 127.4 | 127.7 |
| $C_1 - \widehat{C_2} - C_3$ | 120.0 | 120.4 |
| $C_{1'} - \widehat{C_{2'}} - C_{3'}$ | 120.0 | 120.4 |
| $C_1 - \widehat{C_2} - C_{2'}$ | 108.5 | 109.0 |
| $C_{1'} - \widehat{C_7} = O$ | 127.4 | 127.7 |
| $C_1 - \widehat{C_7} = O$ | 127.4 | 127.7 |
| $C_6 - \widehat{C_1} - C_7$ | 129.2 | 129.5 |
| $C_{6'} - \widehat{C_1} - C_{7'}$ | 129.2 | 129.5 |

The rings formed by the 1–6 and 1′–6′ C-atoms of both the fluorenone molecule and its cation are significantly distorted, compared to the corresponding rings in benzophenone.[8] This is certainly due to the additional C(2)–C(2′) bond in fluorenone, which forces the planarity of the molecule and the subsequent electronic coupling between the rings. The latter is limited in benzophenone because of the repulsion between the hydrogens at the C(2) and C(2′) atoms.

Another effect of the fluorenone rigidity appears when considering the changes in angles between the neutral molecule and its cation. Much smaller changes are observed in fluorenone than in benzophenone, indicating a very small skeleton alteration of this molecule upon ionization. In particular, the fluorenone molecule and its cation have both a $C_{2v}$ geometry, whereas the $C_2$ geometry of the benzophenone molecule is lowered to $C_1$ in the cation.[8]

Concerning the C(7)═O distance, upon ionization, it is shortened from 1.213 to 1.205 Å in fluorenone whereas it is elongated from 1.214 to 1.228 Å in benzophenone. Therefore, both the weight of the $n_0$ and $\pi_0$ orbitals in the electronic configurations and the delocalization of the positive charge act differently in benzophenone and fluorenone upon ionization.

### 3.4 Computed energetics of the fluorenone cation

The excitation energies of the doublet states of the fluorenone cation were calculated at the MRCI level for two geometries: the optimized geometry of its ground cation electronic state and that of the neutral molecule. These energies are added in Table 2 to the adiabatic ionization energy of fluorenone, 8.316 eV (see below).

Table 2 Calculated (Calc.) and experimental (Exp.) transition energies (eV) from the ground state neutral fluorenone molecule to the ground and excited electronic states of the cation ($D_n \leftarrow S_0$). The calculations of the target ion were performed either at the optimized geometry of the neutral molecule (vertical excitation from $S_0$) or at that of the ground state cation ($D_0$). All calculated values include the ZPE correction. The experimental values were obtained from the top of the lowest sub-structure in each band of the SPES of Fig. 5. The experimental results of Centineo *et al.* are given for comparison

| | Cation | Present work | | |
|---|---|---|---|---|
| | Geom. | Calc. | Exp. | Centineo *et al.*[7] |
| $D_0 \leftarrow S_0$ | $S_0$ | 8.50 | 8.370 ± 0.020 | 8.29 |
| | $D_0$ adiabatic | 8.313 | 8.356 ± 0.007 | |
| $D_1 \leftarrow S_0$ | $S_0$ | 9.81 | 9.180 ± 0.007 | 9.15/9.28/9.47 |
| | $D_0$ | 10.04 | | |
| $D_2 \leftarrow S_0$ | $S_0$ | 10.06 | 10.261 ± 0.007 | 10.2 |
| | $D_0$ | 10.27 | | |
| $D_3 \leftarrow S_0$ | $S_0$ | 12.81 | 11.60 ± 0.10 | 12.12/12.65 |
| | $D_0$ | 12.16 | | |
| $D_4 \leftarrow S_0$ | $S_0$ | | 13.800 ± 0.10 | 14.50 |

## 4 Discussion

### 4.1 Ionization thresholds

**Benzophenone.** The adiabatic ionization energy of benzophenone has been calculated by Khemiri *et al.* at the RCCSD(T)/cc-pVDZ level of theory.[8] The prediction, 8.56 eV, was 0.32–0.24 eV lower than the experimental value reported in the same work.

The calculations that are presented here benefit from the recently implemented and substantially more elaborate (R)CCSD(T)-F12 method. This leads to a dramatic improvement of the basis set convergence and therefore to a fuller account of the electronic correlation.[27,42] The corresponding prediction of the adiabatic ionization energy of benzophenone is 8.905 eV, *i.e.* 0.02–0.10 eV higher than the experimental threshold reported by Khemiri *et al.*[8] As expected, this value is closer to the experiment than that reported in ref. 8. Nevertheless, given the improvement mentioned above, we were expecting a better agreement. This prediction is indicated by a green arrow over the benzophenone SPES in Fig. 3. It is only 18 meV lower in energy than the first structure in the spectrum. This pushed us to reconsider the experimental determination of the adiabatic ionization threshold and consider that the rising edge of the SPES at low energy is due to the superposition of congested rovibrational lines. We examine this point below in light of recent work.

A series of SPESs have been reported on medium-size molecules: 3-hydroxyisoquinoline,[30] thymine,[32] cytosine[12] and adenine.[33] A temperature dependent study was performed in the latter example, showing that at increasing temperatures, a tail appears in the rising edge of the SPES. Its width of *ca.* 0.1 eV was discussed as due to hot rovibrational bands because of incomplete vibrational cooling of the neutral molecule in the supersonic expansion. When following

this analysis, and assuming the tail coming from a vibrationally hot ground state, the adiabatic ionization threshold of benzophenone is determined by what we estimate to be the top of the first structure of the SPES. It is measured at 8.923 ± 0.005 eV as shown in Fig. 3. This threshold was erroneously attributed to the vertical ionization threshold by Khemiri *et al.*[8]

Our theoretical prediction of the adiabatic ionization energy of benzophenone (8.905 eV) is only 18 meV lower than our experimental determination (8.923 ± 0.005 eV). The agreement between experiment and calculation is therefore excellent, almost within the experimental uncertainty. The differences may be attributed to the contribution of the core–valence (CV) and scalar relativistic (SR) effects, which are costly to evaluate in molecules such as benzophenone, which contain H, C and O atoms only. This was discussed in the case of cytosine[11,12] and adenine[33] and applies here as well.

**Fluorenone.** The photoionization of fluorenone is most probably a direct ionization process which forms the lowest doublet states of the cation upon removal of an electron from the outermost valence orbitals of the neutral molecule. The same assumption was made implicitly for benzophenone. It is justified by the excellent agreement between calculation and experiment. Hence, as for benzophenone, the width of the rising edge of the fluorenone SPES at low energy reflects a congestion of lines associated with the population of bands corresponding to low frequency modes of the neutral molecule. The latter are populated because of incomplete cooling during the supersonic expansion. With fluorenone, the rising edge is slightly widened by the loss of resolution mentioned in Section 3.2 due to the high energy limit of 120 meV which is given to the photoelectrons used to construct the SPES. This reduces the accuracy of the experimentally determined adiabatic ionization threshold. Taking this into account, and using the criteria defined previously with the benzophenone molecule, the adiabatic ionization threshold is measured to be 8.356 ± 0.007 eV for fluorenone. This value is in agreement, within +43 meV, with the calculated value of 8.313 eV (see Table 2).

The adiabatic ionization energy of fluorenone (8.356 ± 0.007 eV) is smaller than that of benzophenone (8.923 ± 0.005 eV) by 0.567 eV. This is probably related to a stabilization of the fluorenone cation that cannot occur in benzophenone. In the case of the fluorenone cation, the positive charge can resonantly delocalize over the whole molecule *via* the three cycles. In contrast, such charge delocalization is severely limited in benzophenone where the planar symmetry is broken by the repulsion between the H-atoms in the *ortho* position, *i.e.* between the H-atoms that are bonded to the 2 and 2′ C-atoms of benzophenone (see the atom labeling in Fig. 1).

### 4.2 Electronic states of the cations

**Benzophenone.** The black horizontal lines on the left hand side of Fig. 8 recall the calculations of Khemiri *et al.*[8] dealing with the excitation energy of the benzophenone cation at the optimized geometry of the ground doublet state $D_0$. For an easier comparison with the experiment, the adiabatic ionization energy of benzophenone that was calculated in the present work (8.905 eV, see above) is added to the calculation of Khemiri *et al.* in Fig. 8. Finally, we have complemented the Khemiri *et al.* information by calculating the energy of the lowest quartet ionic state $Q_0$ at the same geometry. The PBE0/aug-cc-pVDZ(opt)//(R)CCSD(T)-F12/aug-cc-pVDZ(SP) procedure described above was used. The $Q_0$ state has the same electronic configuration as the $D_4$ state. Its energy is 11.73 eV, *i.e.* 1.01 eV below that of $D_4$.

Fig. 8 shows that no direct photoionization toward a benzophenone doublet state is expected with photon energies ranging between 10.7 and 12.5 eV. When adding hypothetical direct photoionization towards the quartet state, the gap is between 10.7 and 11.7 eV.

**Fluorenone.** The SPES of fluorenone (Fig. 5) is in marked contrast with that of benzophenone. Two bunches of bands, a hat-shape one and a sharper one, are observed with threshold energies at 9.18 eV and 10.26 eV, respectively. These two energies were obtained using the same criteria as for determining the ionization energy. They are reported in Table 2 where they are compared to the present calculations and to the experimental determinations of Centineo *et al.*[7] A good agreement is found between the present experimental thresholds and those reported in the pioneering work of Centineo *et al.* A satisfactory agreement is also observed with the present calculations. It is nevertheless uneven from one excited state to the other. This may simply reflect that the calculations were not performed at the equilibrium geometry of the relevant excited state of the cation but either at the equilibrium geometry of the neutral molecule or at that of the ground state cation. Nevertheless, additional interpretation will be discussed later in the text.

To go further in the discussion, Table 3 lists the dominant electron configuration of the four lowest states of fluorenone. It is provided for two optimized geometries, that of the neutral molecule and that of the ground state cation. The dominant configuration is the same with almost the same weight in both geometries. Hence, the electronic configuration does not change much when distorting the fluorenone cation from one geometry to the other and no surface crossing is expected upon such deformation. In contrast, the excited state energies are

Table 3 Dominant electron configuration (second column with the weight in parentheses) of the four lowest states of the fluorenone cation provided by the IC-MRCI calculation for two geometries of the cation: the optimized geometry of the neutral molecule and that of the ground state cation. H and L are for the HOMO and LUMO respectively. Similar information for benzophenone is available in ref. 8. The $D_0$ state is taken as the energy origin in both geometries

| State | Configuration | Energy (eV) |
|---|---|---|
| Fluorenone$^+$ at the optimized geometry of the ground state neutral | | |
| $D_0$ | $(H-2)^2(H-1)^2(H)^1$ (0.95) | 0 |
| $D_1$ | $(H-2)^2(H-1)^1(H)^2$ (0.93) | 1.31 |
| $D_2$ | $(H-2)^1(H-1)^2(H)^2$ (0.94) | 1.56 |
| $D_3$ | $(H-2)^2(H-1)^2(H)^0(L)^1$ (0.91) | 4.31 |
| Fluorenone$^+$ at the optimized geometry of the ground state cation | | |
| $D_0$ | $(H-2)^2(H-1)^2(H)^1$ (0.96) | 0 |
| $D_1$ | $(H-2)^2(H-1)^1(H)^2$ (0.93) | 1.73 |
| $D_2$ | $(H-2)^1(H-1)^2(H)^2$ (0.93) | 1.96 |
| $D_3$ | $(H-2)^2(H-1)^2(H)^0(L)^1$ (0.93) | 3.85 |

 

affected significantly by about 0.5 eV, indicating that the corresponding PESs have fairly steep slopes at the vertical of the equilibrium geometry of the $S_0$ state.

### 4.3 Dissociative ionization of benzophenone

Action-SPES such as those reported in Fig. 3 and 4 show information similar to the yield of the relevant ion, either the parent (Fig. 3) or a fragment (Fig. 4) in coincidence with its threshold electron. Hence, neglecting the small internal energy of the neutral molecule prior to ionization, the horizontal scale of the action-SPESs represents the sum of the "adiabatic ionization energy" of the neutral molecule (measured here at 8.923 eV) and the "internal energy of the cation". The internal energy of the benzophenone cation is therefore derived from the horizontal scale of Fig. 3 and 4 by simply subtracting the measured adiabatic ionization energy. This, together with the scaling of ion signals in these figures to relative ion intensities, gives access to a breakdown diagram, which shows the relative abundance of the parent cation and fragments as a function of the cation internal energy. Breakdown diagrams are convenient tools for discussing the dynamics of dissociative photoionization.[43,44] The breakdown diagram that was built using the action-SPESs of Fig. 3 and 4 is shown in the top panel of Fig. 7. Three fragmentation channels are observed. The main one is the loss of a phenyl group $C_6H_5$, forming the $C_7H_5O^+$ radical cation. The loss of a CO group (formation of the $C_{12}H_{10}^+$ cation) is always a minor channel. It contributes to less than 3% of the total ion signal in the explored energy range. It is steadily growing above threshold. Finally, the fragmentation channel where a H-atom is lost (formation of $C_{13}H_9O^+$) is significant in a narrow window of the ion internal energy: ~0.20 eV wide centered at 2.4 eV (*i.e.* photon energy ~11.3 eV).

Table 4 and Fig. 8 report the appearance energies measured experimentally (second column) for the three fragmentation channels (first column). As discussed earlier for the fluorenone molecule, extending the range of photoelectron energy when constructing the SPESs leads to a lower energy resolution, especially when unstructured tails are considered. The breakdown diagram shown in the top panel of Fig. 7 was build on SPESs of a wide range from 0 to 1.4 eV of kinetic energy, because of the low signal intensity, which reduces dramatically the energy resolution. As a consequence, the appearance energies were obtained more accurately with the relative ion yield of the fragment ions (without consideration of the electron energy) as displayed in Fig. 7 (bottom panel). The appearance

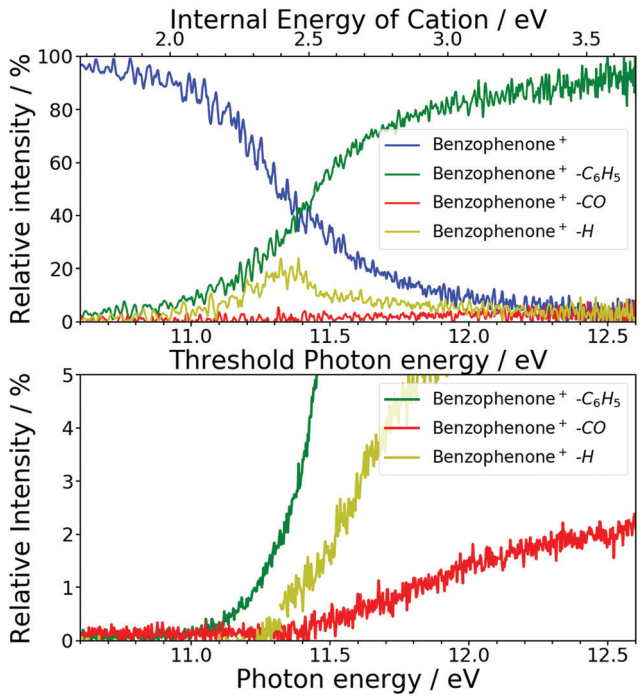


Fig. 7 Breakdown diagrams of the benzophenone cation fragmentation, built from the SPESs of Fig. 3 (top panel) and from the total ion yield of Fig. 4 (bottom panel). The full scale of this last graph is presented in the ESI.† These diagrams are relative and show the passage from parents to fragments.[43,44]

Table 4 For each fragmentation channel (first column), the experimental appearance energy (second column) deduced from the bottom panel of Fig. 7 is compared to the present calculations ($\Delta E_r$ in the third column, see the text for details). Electron impact measurements are reported in the last column for comparison

| | Present work | | Previous work |
|---|---|---|---|
| | Experiment | $\Delta E_r$ calculation | Electron impact |
| $C_7H_5O^+ + C_6H_5$ | 11.04 ± 0.02 | 10.67 | 12.00 ± 0.05[45]<br>11.32 ± 0.1[46] |
| $C_{13}H_9O^+ + H$ | 11.28 ± 0.02 | 13.88/10.93[a] | |
| $C_{12}H_{10}^+ + CO$ | 11.45 ± 0.02 | 8.24 | 12.24 ± 0.13[45] |

[a] The *xx*/*yy* energies correspond to the formation of two isomers of the $C_{13}H_9O^+$ cation (eqn (3)/eqn (4), respectively).

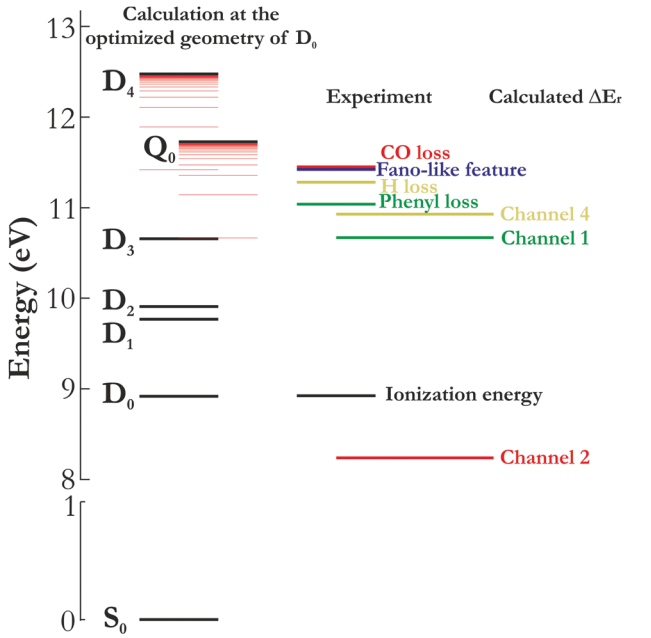


Fig. 8 Energetics of the benzophenone molecule and cation, summarizing calculations and experimental data. The thin red lines simulate Rydberg series (quantum defect $\delta$ = 0.1) converging towards the $D_4$ and $Q_0$ states of the cation. For the fragmentation processes in action, see the text.

energies are estimated from a linear interpolation of the signal onset. Table 4 reveals that the three fragmentation channels have about the same experimental appearance energy, within ±0.2 eV at 11.2 eV. This observation is in fair agreement with the experimental values obtained from electron impact ionization, which are also shown in Table 4 (last column).

Table 4 and Fig. 8 report also the calculated threshold energy of each fragmentation channel ($\Delta E_r$, third column). The calculations follow the PBE0/augcc-pVDZ(opt)//(R)CCSD(T)-F12/aug-cc-pVDZ(SP) procedure described above. The calculated $\Delta E_r$ value of each channel includes the zero point energy and assumes that the neutral benzophenone parent and the relevant neutral and ionic fragments are in their ground electronic states. The exit channel of these dissociations needs a comment since only the mass of the fragment ion is known experimentally and not its structure.

We do not think that ambiguity exists in the structure of the ionic fragments when a phenyl or a CO group is lost. Hence, the bond between the C(7) and C(1) (or C(1′)) atoms is broken in the fragmentation channel 1, whereas the biphenyl radical cation is formed in fragmentation channel 2.

$$C_{13}H_{10}O^+ \rightarrow C_7H_5O^+ + C_6H_5^\bullet \quad \Delta E_r = 10.67 \text{ eV} \qquad (1)$$

$$C_{13}H_{10}O^+ \rightarrow C_{12}H_{10}^{+\bullet} + CO \quad \Delta E_r = 8.24 \text{ eV} \qquad (2)$$

In contrast, several pathways were explored when a H atom is lost. The simplest one is a single bond breaking, C(2)–H (or C(2′)–H), and no bond rearrangement in the fragment ion occurs:

$C_{13}H_{10}O^+ \rightarrow$ 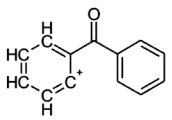 $+ H^\bullet$, $\Delta E_r = 13.88$ eV. (3)

A substantial bond rearrangement is however assumed in the other fragmentation pathways:

$C_{13}H_{10}O^+ \rightarrow$ 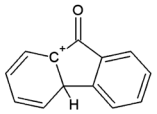 $+ H^\bullet$, $\Delta E_r = 10.93$ eV. (4)

$C_{13}H_{10}O^+ \rightarrow$ 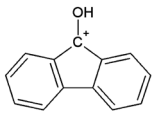 $+ H^\bullet$, $\Delta E_r = 9.35$ eV. (5)

The comparison between the theoretical information on $\Delta E_r$ and the experimental appearance energies in Table 4 and Fig. 8 is extremely surprising. The latter do not vary very much from one fragmentation channel to the other, whereas substantial differences appear in the calculations. In our opinion this is the fingerprint that a complex dynamics is at play. In the following, each channel is examined in depth.

**Loss of $C_6H_5$.** This is the main fragmentation channel. The simplest assumption regarding its mechanism is the single bond breaking provided by reaction channel 1. It is consistent with the predicted equilibrium geometry of the ground state benzophenone ion where the two phenyl groups are not equivalent (the $C_2$ symmetry is broken in the ion).[8] This channel does not require a substantial rearrangement of the fragment ion that is formed and is therefore associated with a fairly simple dynamics. Not surprisingly, the experimental appearance energy of this channel (11.04 eV, see Table 4) is close to the calculated value ($\Delta E_r$ = 10.67 eV). Nevertheless, the experimental value is 0.37 eV larger than the calculated one (compare the two horizontal green curves in Fig. 8 or the numbers in Table 4). Given the expected accuracy of the calculations, we consider that this difference is the fingerprint of a barrier of *ca.* 0.4 eV along this fragmentation pathway.

**Loss of H.** The second important fragmentation channel is the loss of a H atom. The experimental appearance energy is 11.28 ± 0.02 eV and the channel is significant within a narrow energy window of 0.2 eV. This uncommon behavior may explain why this channel was not observed in previous work where electron impact ionization was performed.[45,46] It suggests a complex dynamics. The predicted value of $\Delta E_r$ along the fragmentation channel 3 is more evidence of this complexity. This pathway assumes indeed an oversimple dynamics where a single bond is broken while a much larger appearance energy is predicted than that observed experimentally (13.88 *versus* 11.28 eV). This difference is far larger than the expected calculation inaccuracies, an indication that this scheme does not properly describe the loss of a H atom. Actually, we suspect that fragmentation pathways exist where internal bond rearrangements in the cation reduce $\Delta E_r$. Without exploring extensively the potential energy surface of the radical cation, reaction channels 4 and 5 propose two plausible pathways where the calculated $\Delta E_r$ value is consistent with the experiment. In terms of kinetics, the more endoenergetic reaction channel 4 seems more favored than channel 5, which requires a more extensive bond rearrangement. In reaction channel 4, indeed, the H-loss is simply accompanied by the formation of the C(2)–C(2′) bond and appears as a preliminary step leading to reaction channel 5, but after the migration of the H atom. This pathway is that reported in Fig. 8. Other reaction channels which are associated with larger $\Delta E_r$ values are presented in the ESI.†

**Loss of CO.** The appearance energy of the biphenyl cation, 11.45 eV, is far above the calculated value of 8.24 eV. Again we do not consider that such a large difference is due to inaccuracies in the calculation. Instead, it suggests that this fragmentation channel must overcome a barrier, ∼ 11.45–8.24 = 3.21 eV above the energy of the products. This is actually not surprising since the CO-loss requires the simultaneous breaking of two bonds and the formation of a new one.

After crossing the barrier, the potential energy surface of the benzophenone cation decreases by 3.21 eV when reaching full dissociation. Likely, a substantial fraction of this energy is transferred as kinetic energy of the $C_{12}H_{10}^+$ (mass 154 u) and CO fragments. This is consistent with the observation of a very broad peak at 154 u in Fig. 2.

### 4.4 Tentative unified mechanism of the benzophenone fragmentation

The former section showed that the calculated adiabatic threshold energies of the fragmentation channels 1–5 are substantially

different from one another. In contrast, the measured appearance energies for the loss of a $C_6H_5$, H or CO group are comparable, within 0.4 eV (see Table 4). The most intriguing situations are met with the loss of H and that of CO. Both are associated with a complex dynamics which implies the rearrangement of several bonds and their experimental appearance energies (11.28 and 11.45 eV, respectively) are within 0.17 eV. The measured appearance energy of the other fragmentation channel is slightly lower in energy, 11.04 eV. It is the dominant fragmentation channel and corresponds to a fairly simple dynamics where the $C_6H_5$ group is lost in a single bond breaking. It is striking to notice that the appearance energy of these three channels falls in the 10.7–11.7 eV gap mentioned in Section 4.2 where no direct transition to the benzophenone cation (either in doublet or quartet states) is expected. Hence, if these fragmentation channels were opened upon direct photoionization to one of these states, this would require a very deformed geometry of either neutral or cationic benzophenone. The photoionization would therefore proceed far from the Franck–Condon region and the relevant fragment ion would hardly appear with a well identified threshold behaviour as observed in Fig. 4 with the loss of $C_6H_5$ (green curve).

This question is discussed further now when bringing together the sudden rise of the full-SPES in Fig. 3 with the Fano-like profile of the action-SPES. Both occur at the same energy, at $11.421 \pm 0.010$ eV. This observation is surprising and informative in several aspects.

Firstly, when considering the appearance energy of the fragmentation channels as we did above, $11.421 \pm 0.010$ eV falls in the gap where no direct photoionization is expected. Given the steepness of the rise observed in the full-SPES of Fig. 3, photoionization far from the Franck–Condon region can hardly be invoked. The same conclusion was drawn just above when considering fragmentation.

Secondly, a specific feature of the sharp increase of the full-SPES is the near coincidence with the appearance energy of the fragmentation channels (especially the CO loss, see Fig. 8). An analogy can be made with the steep rise at the fragmentation threshold which has been reported in the total photo-electron signal in Pulse Field Ionization (PFI-PE) experiments where, *e.g.*, $ND_3^{+}$[47] or $CH_4^{+}$[48] ions are formed.[49] The interpretation of the PFI experiments is based on the intermediate excitation of high Rydberg states, the fragments of which, appearing at a lower energy than the one of the ion, form a reservoir that is subsequently ionized by a pulsed electric field when the threshold energy is reached. The steep rise was interpreted by these authors as revealing a competition between two fragmentation pathways, one along the parent ion energy surface (a′–d) in scheme (6) and the other along the neutral intermediate Rydberg surface (a–c), which can be followed by (e) when the internal energy required is reached.

$$\begin{array}{lcccc} \text{Parent} + h\nu & \xrightarrow{(a')} & \text{Parent}^{\star +} & \xrightarrow{(d)} & \text{Fragment}^{+} \\ & (a)\searrow & (b)\uparrow & & (e)\uparrow \\ & & \text{Parent}^{\star\star} & \xrightarrow{(c)} & \text{Fragment}^{\star} \\ & & & & (f)\downarrow \\ & & & & \text{Fragment} \end{array} \quad (6)$$

Applying the reaction diagram 6 to the present context of a SPES experiment, the direct ionization pathway (a′) is always open since the photon energy is much larger than the ionization energy. Actually, several direct ionization pathways are opened when the photon energy reaches the region above 11 eV (see Fig. 8). This (these) pathway(s) may compete and interfere with one or several autoionization pathways involving Rydberg states. High autoionizing Rydberg states may be present and can be excited as exemplified by Briant *et al.*[10] for the argon dimer. To substantiate this anticipation, two Rydberg series converging to the $D_4$ and $Q_0$ states of the benzophenone cation are drawn in Fig. 8 (thin red lines), assuming a quantum defect $\delta = 0.1$ (arbitrarily chosen). We do not claim to assign here a such resonance. The important point is elsewhere. These doubly excited Rydberg series are especially relevant in the present context because the core electron configuration of the $D_4$ and $Q_0$ states involves the promotion of two non bonding HOMO electrons into at least an anti-bonding one, the LUMO orbital, which has a $\pi^*_{CO}$ character.[8] Such a $n^{-2}\pi^*_{CO}X^*$ configuration is likely to drive fragmentation. Accordingly, an autoionization pathway would be associated with the pathways (b) and (e) in scheme (6) whether the parent Rydberg or an excited fragment autoionizes. In a SPES experiment as here, competing and therefore interfering pathways would exist for forming the parent ion: (a′) and (a–b). Competing pathways would also exist for forming the fragment ions: (a′–d) and (a–c–e). Having this in mind, the appearance energy of the fragmentation channels listed in Table 4 and the Fano-like profile observed at $11.421 \pm 0.010$ eV in the action-SPES for forming the parent ion (see Fig. 3) are tentatively attributed to the fingerprint of the competition (interference) between direct photoionization and pathways going through the excitation of one or several autoionizing Rydberg states.

Note, however, that the energetics along such pathways is severely constrained. The main difference between the fragmentation pathway occurring on the ionic or the neutral potential energy surface is the amount of energy involved to fragment or reorganize the molecular structure. Indeed, the extra energy, which is the ionization energy of the parent molecule, is sufficient to overcome very fast standard barriers for bond breaking. The channel (c) is also efficient, even below the expected reaction energy invoked in the previous section, but then, the thermodynamics prevents the occurrence of channel (e). When the total energy furnished by the photon is large enough to open the channel (e), the reservoir of Fragment* is open to detection, whereas Parent** was depleted by channel (c). For this reason, generalized from the PFI-PE experiments,[48] the appearance of fragments leads to a large increase of the total cross section as observed in Fig. 3.

Moreover, since the barriers for (d) and (c) are not overcome under the same energetic condition, as mentioned previously, competitive ionization dynamics are expected. Indeed, the experimental observations can be fully interpreted if the (d) channel is blocked. In a such scheme, the benzophenone cation issued from (a′) coexists with its fragments even above the first fragmentation threshold, as the formation of the fragment is derived only from the (c) pathway. Furthermore, (c) competes with (b) leading to the same

product as (a′) through a different pathway. The benzophenone cation signal shows also a Fano profile.

At least, such interpretation explains the mismatch observed between the excited state energy calculated and the structure of the SPES spectrum for both molecules investigated. Especially here, the $D_1$ state of fluorenone shows experimentally an unexpected structure that is strongly shifted from the theoretical value estimated. Although the computed value is not calculated at the optimal geometry of this excited state, the structures can be attributed to a (a–b) ionization scheme.

# 5 Summary and conclusion

Single photon ionization and subsequent unimolecular decomposition of jet-cooled benzophenone and fluorenone were studied at synchrotron SOLEIL using the VUV beamline DESIRS coupled to a photoion/photoelectron coincidence setup (SAPHIRS setup + DELICIOUS III spectrometer). The experimental information was deduced from Slow PhotoElectron Spectroscopy (SPES), which document the photoionization cross-section at a fixed ion energy as a function of its threshold photon energy. Two kinds of SPESs were presented where either the electrons are recorded or only those in coincidence with ions of a specific mass. The former are called full-SPESs and the latter action-SPESs.

Single photon ionization and subsequent unimolecular decomposition of jet-cooled benzophenone and fluorenone were studied at synchrotron SOLEIL using the VUV beamline DESIRS coupled to a photoion/photoelectron coincidence setup (SAPHIRS setup + DELICIOUS III spectrometer). The experimental information was deduced from Slow PhotoElectron Spectroscopy (SPES), which document the photoionization cross-section at a fixed ion energy as a function of its threshold photon energy. Two kinds of SPESs were presented where either the electrons are recorded or only those in coincidence with ions of a specific mass. The former are called full-SPESs and the latter action-SPESs.

SPESs were recorded over the 8.5–12.7 eV and 8.2–14.2 eV photon energy range for benzophenone and fluorenone, respectively. Dissociative ionization is observed for benzophenone only. The full interpretation of the measurements, including the identification of the neutral and ionic fragments when dissociative ionization is at play, benefits from high level *ab initio* computations. These provide us with the equilibrium structures and energetics of the neutral and ionized molecules and of their ionized fragments. Electronically excited states of the parent molecular ions were calculated for fluorenone when this information was not yet available. We have a reasonably good agreement for the $D_0$, $D_2$ and $D_3$ bands. Our computed energy for $D_1$ matches the third component of the corresponding band. So maybe autoionisation, which is in action in the present system, contributes to the population of these two unattributed structures.

A careful comparison between the SPES of benzophenone and our calculations led us to reconsider the experimental determination of the adiabatic ionization energy of this molecule, now determined to be 8.923 ± 0.005 eV. The same quantity was measured to be 8.356 ± 0.007 eV for fluorenone. Both measurements are in excellent agreement with the calculations, almost within the experimental uncertainty.

The appearance energies of the benzophenone fragment ions were determined at 11.04 ± 0.02 eV (loss of $C_6H_5$), 11.28 ± 0.02 eV (loss of H) and 11.45 ± 0.02 eV (loss of CO). Comparison with the predicted reaction thresholds for these channels reveals a complex dynamics. A small exit barrier of 0.37 eV was identified along the pathway where $C_6H_5$ is lost, nevertheless this channel is fairly direct since only a single bond is broken and no substantial bond rearrangement of the fragments takes place. This is not the case for the loss of H, where the molecular structure of the ionic fragment $C_{13}H_9O^+$ is strongly rearranged. Even more complex is the dynamics which leads to the loss of CO. Two chemical bonds are broken, a new one is formed and the reaction goes through a transition state which is 3.21 eV above the expected dissociation limit; a substantial fraction of this excess energy is shared as kinetic energy in the $C_{12}H_{10}^+$ and CO fragments. Apparently, the dynamics forming the parent cation and its fragments involves members of the doubly excited Rydberg series converging toward excited states of the cation near the $D_4$ and $Q_0$ states. The proposed mechanism needs to be confirmed by further experimental and theoretical investigations.

To conclude, we consider firstly that the present work illustrates the high level of confidence that can be placed in the energetics of medium size molecules and molecular ions when predicted by the following composite calculation scheme: optimization of molecular structures at the PBE0/aug-cc-pVDZ level; and single point energy calculations at the (R)CCSD(T)-F12/aug-cc-pVDZ level. To state this, we do not consider only the present work on benzophenone and fluorenone but also the series of studies on 3-hydroxyisoquinoline,[30] thymine,[32] cytosine[12] and adenine.[33] This work on benzophenone is also a step to establish the power of this composite calculation scheme to help understand the complex dynamics ongoing in the cation. None of our previous studies, nor the present one on fluorenone, was considering floppy systems such as benzophenone, its ion and fragments and therefore systems where complex dynamics are so difficult to unravel. Secondly, the present work indicates the dramatic effect of the molecular dynamics of autoionizing states on the ionization and fragmentation dynamics of large molecules. Actually it extends the previous observations focused exclusively on such dynamics by PFI experiments to the general case where autoionizing dynamics competes efficiently with direct ionization caused processes, up to dominating them. Such pre-ionizing fragmentation is unlikely limited to the lone benzophenone molecule and is actually expected to be present, at various degrees of importance, at least in large organic molecules.

# Conflicts of interest

There are no conflicts to declare.

# Acknowledgements

We acknowledge access to the Synchrotron Soleil facility under project No. 20120540 and 20160859. We thank Dr Laurent

Nahon, DESIRS beamline director, Dr Gustavo Garcia and Jean-François Gil for assistance in using the beamline DESIRS. Partial support was received from the seventh European Community Framework Program under COST ACTION CM1405 MOLIM. AR thanks the Deutsche Forschungsgemeinschaft, Research Training School, GRK 2112 ''Molecular Biradicals: Structure, Properties and Reactivity'' for financial support.

## References

1 R. M. Hochstrasser, H. Lutz and G. W. Scott, *Chem. Phys. Lett.*, 1974, **24**, 162–167.
2 S. Aloise, C. Ruckebusch, L. Blanchet, J. Rehault, G. Buntinx and J. P. Huvenne, *J. Phys. Chem. A*, 2008, **112**, 224–231.
3 G. Spighi, M.-A. Gaveau, J.-M. Mestdagh, L. Poisson and B. Soep, *Phys. Chem. Chem. Phys.*, 2014, **16**, 9610–9618.
4 B. Soep, J. M. Mestdagh, M. Briant, M. A. Gaveau and L. Poisson, *Phys. Chem. Chem. Phys.*, 2016, **18**, 22914–22920.
5 J. Koehler, P. Hemberger, I. Fischer, G. Piani and L. Poisson, *J. Phys. Chem. A*, 2011, **115**, 14249–14253.
6 L. Favero, G. Granucci and M. Persico, *Phys. Chem. Chem. Phys.*, 2016, **18**, 10499–10506.
7 G. Centineo, I. Fragala, G. Bruno and S. Spampinato, *J. Mol. Struct.*, 1978, **44**, 203–210.
8 N. Khemiri, S. Messaoudi, M. Abderrabba, G. Spighi, M. A. Gaveau, M. Briant, B. Soep, J. M. Mestdagh, M. Hochlaf and L. Poisson, *J. Phys. Chem. A*, 2015, **119**, 6148–6154.
9 J. C. Poully, J. P. Schermann, N. Nieuwjaer, F. Lecomte, G. Gregoire, C. Desfrancois, G. A. Garcia, L. Nahon, D. Nandi, L. Poisson and M. Hochlaf, *Phys. Chem. Chem. Phys.*, 2010, **12**, 3566–3572.
10 M. Briant, L. Poisson, M. Hochlaf, P. de Pujo, M.-A. Gaveau and B. Soep, *Phys. Rev. Lett.*, 2012, **109**, 193401.
11 M. Hochlaf, *Phys. Chem. Chem. Phys.*, 2017, **19**, 21236–21261.
12 Z. Chen, K.-C. Lau, G. A. Garcia, L. Nahon, D. K. Božanić, L. Poisson, M. M. Al-Mogren, M. Schwell, J. S. Francisco, A. Bellili and M. Hochlaf, *J. Am. Chem. Soc.*, 2016, **138**, 16596–16599.
13 L. Nahon, N. de Oliveira, G. A. Garcia, J.-F. Gil, B. Pilette, O. Marcouille, B. Lagarde and F. Polack, *J. Synchrotron Radiat.*, 2012, **19**, 508–520.
14 M. Richard-Viard, A. Delboulbé and M. Vervloet, *Chem. Phys.*, 1996, **209**, 159.
15 G. A. Garcia, B. K. C. de Miranda, M. Tia, S. Daly and L. Nahon, *Rev. Sci. Instrum.*, 2013, **84**, 053112.
16 T. Baer and R. P. Tuckett, *Phys. Chem. Chem. Phys.*, 2017, **19**, 9698–9723.
17 G. A. Garcia, L. Nahon and I. Powis, *Rev. Sci. Instrum.*, 2004, **75**, 4989–4996.
18 T. Barillot, R. Brédy, G. Celep, S. Cohen, I. Compagnon, B. Concina, E. Constant, S. Danakas, P. Kalaitzis, G. Karras, F. Lépine, V. Loriot, A. Marciniak, G. Predelus-Renois, B. Schindler and C. Bordas, *J. Chem. Phys.*, 2017, **147**, 013929.
19 C. Adamo and V. Barone, *J. Chem. Phys.*, 1999, **110**, 6158–6170.
20 M. J. Frisch, G. W. Trucks, H. B. Schlegel, G. E. Scuseria, M. A. Robb, J. R. Cheeseman, G. Scalmani, V. Barone, B. Mennucci, G. A. Petersson, H. Nakatsuji, M. Caricato, X. Li, H. P. Hratchian, A. F. Izmaylov, J. Bloino, G. Zheng, J. L. Sonnenberg, M. Hada, M. Ehara, K. Toyota, R. Fukuda, J. Hasegawa, M. Ishida, T. Nakajima, Y. Honda, O. Kitao, H. Nakai, T. Vreven, J. A. Montgomery Jr., J. E. Peralta, F. Ogliaro, M. J. Bearpark, J. Heyd, E. N. Brothers, K. N. Kudin, V. N. Staroverov, R. Kobayashi, J. Normand, K. Raghavachari, A. P. Rendell, J. C. Burant, S. S. Iyengar, J. Tomasi, M. Cossi, N. Rega, N. J. Millam, M. Klene, J. E. Knox, J. B. Cross, V. Bakken, C. Adamo, J. Jaramillo, R. Gomperts, R. E. Stratmann, O. Yazyev, A. J. Austin, R. Cammi, C. Pomelli, J. W. Ochterski, R. L. Martin, K. Morokuma, V. G. Zakrzewski, G. A. Voth, P. Salvador, J. J. Dannenberg, S. Dapprich, A. D. Daniels, Ö. Farkas, J. B. Foresman, J. V. Ortiz, J. Cioslowski and D. J. Fox, *Gaussian 09, Revision A.02*, 2009.
21 T. H. Dunning, *J. Chem. Phys.*, 1989, **90**, 1007–1023.
22 R. A. Kendall, T. H. Dunning and R. J. Harrison, *J. Chem. Phys.*, 1992, **96**, 6796–6806.
23 Y. Tantirungrotechai, K. Phanasant, S. Roddecha, P. Surawatanawong, V. Sutthikhum and J. Limtrakul, *THEOCHEM*, 2006, **760**, 189–192.
24 H.-J. Werner, P. J. Knowles, G. Knizia, F. R. Manby and M. Schütz, *Wiley Interdiscip. Rev.: Comput. Mol. Sci.*, 2012, **2**, 242–253.
25 G. Knizia, T. B. Adler and H.-J. Werner, *J. Chem. Phys.*, 2009, **130**, 054104.
26 T. B. Adler, H.-J. Werner and F. R. Manby, *J. Chem. Phys.*, 2009, **130**, 054106.
27 T. B. Adler, G. Knizia and H.-J. Werner, *J. Chem. Phys.*, 2007, **127**, 221106.
28 T. B. Adler and H.-J. Werner, *J. Chem. Phys.*, 2009, **130**, 241101.
29 K. E. Yousaf and K. A. Peterson, *J. Chem. Phys.*, 2008, **129**, 184108.
30 Y. Pan, K.-C. Lau, L. Poisson, G. A. Garcia, L. Nahon and M. Hochlaf, *J. Phys. Chem. A*, 2013, **117**, 8095–8102.
31 Y. Pan, K.-C. Lau, M. M. Al-Mogren, A. Mahjoub and M. Hochlaf, *Chem. Phys. Lett.*, 2014, **613**, 29–33.
32 Y. Majdi, M. Hochlaf, Y. Pan, K. C. Lau, L. Poisson, G. A. Garcia, L. Nahon, M. M. Al-Mogren and M. Schwell, *J. Phys. Chem. A*, 2015, **119**, 5951–5958.
33 H. Y. Zhao, K.-C. Lau, G. A. Garcia, L. Nahon, S. Carniato, L. Poisson, M. Schwell, M. M. Al-Mogren and M. Hochlaf, *Phys. Chem. Chem. Phys.*, 2018, **20**, 20756–20765.
34 I. Derbali, H. R. Hrodmarsson, Z. Gouid, M. Schwell, M.-C. Gazeau, J.-C. Guillemin, M. Hochlaf, M. E. Alikhani and E.-L. Zins, *Phys. Chem. Chem. Phys.*, 2019, DOI: 10.1039/C8CP06751A.
35 P. J. Knowles and H.-J. Werner, *Chem. Phys. Lett.*, 1985, **115**, 259–267.
36 H.-J. Werner and P. J. Knowles, *J. Chem. Phys.*, 1985, **82**, 5053.
37 P. J. Knowles and H.-J. Werner, *Chem. Phys. Lett.*, 1988, **145**, 514–522.

38 H.-J. Werner and P. J. Knowles, *J. Chem. Phys.*, 1988, **89**, 5803–5814.
39 K. R. Shamasundar, G. Knizia and H.-J. Werner, *J. Chem. Phys.*, 2011, **135**, 054101.
40 B. Sztaray, A. Bodi and T. Baer, *J. Mass Spectrom.*, 2010, **45**, 1233–1245.
41 E. J. McAlduff and D. L. Bunbury, *J. Electron Spectrosc. Relat. Phenom.*, 1979, **17**, 81–89.
42 H. J. Werner, G. Knizia, T. B. Adler and O. Marchetti, *Z. Phys. Chem.*, 2010, **224**, 493–511.
43 J. Mähnert, F. Güthe and K.-M. Weitzel, *Ber. Bunsen-Ges.*, 1996, **100**, 1899–1905.
44 G. K. Jarvis, K.-M. Weitzel, M. Malow, T. Baer, Y. Song and C. Y. Ng, *Rev. Sci. Instrum.*, 1999, **70**, 3892–3906.
45 P. Natalis and J. L. Franklin, *J. Phys. Chem.*, 1965, **69**, 2943.
46 P. Krenmayr, R. Heller and K. Varmuza, *Org. Mass Spectrom*, 1974, **9**, 998–1005.
47 M. Hochlaf, J. Palaudoux and A. Ben Houria, *Transworld Research Network*, 2004.
48 Y.-C. Chang, B. Xiong, D. H. Bross, B. Ruscic and C. Y. Ng, *Phys. Chem. Chem. Phys.*, 2017, **19**, 9592–9605.
49 K.-M. Weitzel, G. K. Jarvis, M. Malow, T. Baer, Y. Song and C. Y. Ng, *Phys. Rev. Lett.*, 2001, **86**, 3526–3529.

 